

The 111 and 129 GeV γ -ray lines from annihilations in the Milky Way dark matter halo, dark disk and subhalos

Ilias Cholis,^{1,*} Hani Nurbianto Santosa,^{2,3,†} Maryam Tavakoli,^{4,‡} and Piero Ullio^{2,3,§}

¹*FNAL, Theoretical Astrophysics Group, Batavia, Illinois, 60510, USA*

²*SISSA, Via Bonomea, 265, 34136 Trieste, Italy*

³*INFN, Sezione di Trieste, Via Bonomea 265, 34136 Trieste, Italy*

⁴*II. Institut für Theoretische Physik, Universität Hamburg, Luruper Chaussee 149, 22761 Hamburg, Germany*

(Dated: March 26, 2013)

Recently a series of indications have been put forward suggesting the presence of two γ -ray lines at 110-130 GeV (centered at 111 and 129 GeV). Signals of these lines have been observed toward the Galactic center, at some galaxy clusters and among some of the unassociated point sources of the 2 years Fermi catalogue. Such a combination of signals could be generated by dark matter annihilations in the main dark matter halo, its substructures and nearby galaxy clusters. We discuss here the consistency between the number of events observed at the line energies in the sky and the predictions using results from the Via Lactea II numerical simulation and extrapolations below its mass resolution, taking into account that the annihilation cross-section to the lines can be estimated from the Galactic center signal. We find that some extrapolations to small substructures can naturally account for the point sources signal, although the hypothesis of background only cannot be rejected. We also study the morphology of the γ -ray sky at the 2 lines energies, testing different Galactic diffuse background models to account for interstellar medium uncertainties, and different assumptions on the DM diffuse component profile. We find from template fits that within reasonable diffuse background uncertainties the presence of a spherical halo component is preferred and that cuspy dark matter halo profiles are also preferable even from the full sky fit. We finally check the impact of a dark disk component, suggested by cosmological simulations that include baryons and find that thin dark disks can not be disfavored, thus possibly accounting for the preferentially closer to the Galactic disk distribution of the point sources lines signal.

I. INTRODUCTION

The possible identification by the *Fermi* Gamma-ray Space Telescope of a signal compatible with the monochromatic photon emission due to pair annihilations of cold dark matter (DM) particles has recently been one of the most debated topics. Originally, [1] has suggested the detection of a line at $129.8 \pm 2.4^{+7}_{-13}$ GeV with a 3.3σ significance in a wide window toward the Galactic center (GC). A similar signal has been indicated by [2] at 127.0 ± 2.0 GeV with 5.0σ significance. A pair of lines with energies of 110.8 ± 4.4 and 128.8 ± 2.7 GeV can alternatively explain γ -ray excess with 5.4σ significance [2]. Similarly the line signal at $\simeq 130$ GeV has also been found by [3] with [4–6] suggesting the presence of 2 lines at $\simeq 110$ and 130 GeV. Both line signals are in agreement with constraints from line searches of the *Fermi* collaboration [7] and indicate a preference for dark matter (DM) annihilation rather than decay [1, 2, 8, 9]. The *Fermi* collaboration, motivated by the results of [1–6],

has performed an analysis oriented toward the GC and some of those results are presented in [10, 11]. Similar to [12, 13], no obvious systematic error has been found to account for the amplitude of the line signal measured by [1, 2] (see though [14]). The *Fermi* results confirm a line-like signal at $E \simeq 130$ GeV at 4σ , or $E \simeq 135$ GeV at 3.3σ after reprocessing the data to take into account the shift of the reconstructed energy with time. Yet, some part of the amplitude may be related to limb photons [10]. Adding information on the performance of the instrument's energy reconstruction decreases the significance of the signal [11]. Thus a conclusive answer on whether the line signal is a systematic error identified toward the GC or a signal of DM annihilations, has not been provided yet.

A monochromatic gamma-ray flux is expected in most scenarios in which DM is in the form of weakly interacting massive particles (WIMPs), since two-body annihilation final states containing photons arise at the 1-loop level. At the same time, in such a framework, it is foreseen that tree-level WIMP annihilations into other SM final states, in turn hadronizing and/or decaying into p , \bar{p} , e^\pm , ν s and γ s, would give sizable yields with continuum energy spectrum on top of the monochromatic γ -ray yield. Yet, no clear indication of γ -ray excess, other than the lines, has been found toward the inner few degrees of

*Electronic address: cholis@fnal.gov

†Electronic address: santosa@sissa.it

‡Electronic address: maryam.tavakoli@desy.de

§Electronic address: ullio@sissa.it

the GC, leading to the extraction of constraints on the continuum [5, 15–17].

Another aspect of a WIMP annihilation signal is that one should expect to see line signals at the same energy and annihilation cross-section toward other dark matter targets. In [18], a 130 GeV line signal toward known galaxy clusters has been suggested. There have been also indications for two lines at 111 and 129 GeV in unassociated point sources which would imply the DM annihilation in substructures [19, 20] [61] (see also [21] for an alternative interpretation).

We assume that the line signal from the unassociated point sources is indeed of DM origin with the same annihilation cross-section to the lines as is estimated from the GC. We then confront that signal with predictions from cosmological simulations such as Via Lactea [22–24]. In section II, we discuss the γ -ray data that we use and our general assumptions for the background and the DM density distribution in the Galaxy. As a general reference we use the total number of γ -ray events with energy 111 ± 5 GeV and 129 ± 6 GeV. These events are taken to be of both DM and diffuse/point source γ -ray background origin. The comparison of the observed γ -ray data with the predicted contribution from substructures within the Galaxy’s virial radius is done in section III. Our aim is to conclude on whether the line signal of point sources can be physically associated to the same energy line signal toward the GC and under what assumptions on the substructure distribution. On the CDM simulation side we use VLII subhalo distribution data [24] and also extrapolate the VLII simulation mass function to smaller subhalo masses.

The observed non-isotropic distribution of DM line(s) point sources in the sky could be explained by the presence of a strong dark disk. Such a dark disk would also have an impact on the diffuse distribution of the DM originated line photons. To study the diffuse γ -ray sky at the energies of the 2 lines, one needs predictions on both the Galactic diffuse backgrounds and on the DM diffuse contribution. In section IV, we test that possible contribution to the two γ -ray lines from DM annihilations in the Galaxy and diffuse backgrounds by doing a template fit. The importance of template fits is that one can take into account the different morphologies of the various diffuse components. We study the impact on the significance of a DM signal on the 4π sky (including the GC) of different assumptions for the Galactic diffuse background, related to physical properties of the interstellar medium. We also test different assumptions (and thus different templates) on the main spherical halo density profile, on the significance of the dark disk component to the local dark matter density and its thickness and finally on the contribution of the dimmer DM subhalos that would also add to the diffuse γ -ray sky. We consider that the main contribution from the brighter DM structures have been already observed by [19] and exclude them from the γ -ray fits. We also derive upper limits on the diffuse emission from annihilations in the main DM halo, and give our

conclusions in section V.

II. GAMMA-RAY DATA, DIFFUSE BACKGROUND AND DM DISTRIBUTION ASSUMPTIONS

The *Fermi* Large Area Telescope publicly available events are categorized in different classes based on the expected level of cosmic ray (CR) contamination. In this work we use the ULTRACLEAN events class which is the cleanest γ -ray events sample. There are 686(744) photons with energy between 111 ± 5 GeV and 611(668) photons with energy between 129 ± 6 GeV in the 4 yr (4.4 yr) full sky *Fermi* ULTRACLEAN class γ -ray data, with the quoted energy ranges representing the relevant energy dispersion for these lines [62]. In section III where we compare with the findings of [19], we use the 4yr sample since it approximates their events sample, while in section IV we use the slightly longer period of 4.4 yr.

The emission of the diffuse Galactic γ -ray background above 100 GeV is dominated by the π^0 contribution, i.e. the decay of mesons produced by inelastic collisions of CRs with the interstellar medium (ISM) gas, and by the up-scattering of low energy photons of the interstellar radiation field (ISRF) from high energy CR electrons (inverse Compton scattering). The morphology of these components on the sky is different mainly because of different morphologies of the ISM gas density and the ISRF energy density in the Galaxy. Moreover the energy loss of CR electrons and protons during their propagation in the Galaxy is different. The bremsstrahlung radiation of CR electrons at these energies is completely subdominant but it is included in our code.

To compute the diffuse γ -ray background, we use the DRAGON package [25–27] with a new ISM gas model [28] that ensures good agreement with γ -ray spectral data between 1 and 200 GeV in the full sky and subsections of it [29]. We ignore the contribution of the “dark gas” (not related to DM substructures) whose uncertainties are significant in the inner 5° in latitude [30, 31]. Based on the relevant uncertainties (see [29]), we allow for different assumptions on the ISM gas and the ISRF which influence the π^0 and the inverse Compton γ -ray emissivities respectively.

In the case where there are 2 lines as has been indicated by [2, 4], the energy of these lines is centered at 128.8 ± 2.7 and 110.8 ± 4.4 GeV [2]. The lines come from either the combination of 2γ & $Z\gamma$ lines or from the $Z\gamma$ & $h\gamma$ lines.

In [17], five individual modes/channels of DM annihilation: $\chi\chi \rightarrow W^+W^-$, $\chi\chi \rightarrow b\bar{b}$, $\chi\chi \rightarrow \tau^+\tau^-$, $\chi\chi \rightarrow \mu^+\mu^-$ and $\chi\chi \rightarrow e^+e^-$ have been studied. The limits on the DM annihilation cross-sections based on their contribution to the continuum γ -rays spectrum in the $|l| < 5^\circ$, $|b| < 5^\circ$ observation window have been derived. Typically, DM models have sizable branching ratios into more than one of these channels. Yet apart from the $\chi\chi \rightarrow \mu^+\mu^-$ channel and mainly the $\chi\chi \rightarrow e^+e^-$

channel, in all the other annihilation channels to SM particles with a continuum spectrum, the γ -ray DM signal at 111 and 129 GeV can not be explained/mimicked by the continuum spectrum. Thus it originates from the annihilation into $Z\gamma$ and 2γ . For $\chi\chi \rightarrow e^+e^-$ and $\chi\chi \rightarrow \mu^+\mu^-$, the final state radiation (FSR) and virtual internal bremsstrahlung (VIB) can contribute to the line signal as discussed in [17, 32].

For simplicity we assume that the DM induced γ -rays with energy 111 ± 5 GeV and 129 ± 6 GeV come from the annihilation of a 129 GeV DM particle into $Z\gamma$ and 2γ respectively. Alternatively, these γ -ray lines could come from $h\gamma$ and $Z\gamma$ for the case of a 142 GeV DM particle. The relevant ratio of the luminosity of two lines is taken to be 1/2 for the 111/129 GeV lines as suggested in [19], thus, for the case of 129 GeV DM particle, the annihilation cross-sections to $Z\gamma$ and 2γ are assumed to be the same.

For the DM distribution we assume that it is a combination of a spherically symmetric "main" DM halo and a dark disk (DD). For the main halo we assume a spherical Einasto DM profile:

$$\rho_{sph}(r) = \rho_{Ein} \exp \left\{ -\frac{2}{\delta} \left[\left(\frac{r}{r_c} \right)^\delta - 1 \right] \right\}, \quad (1)$$

using $\delta = 0.13, 0.17, 0.22$ [33] with $r_c = 20$ kpc. The values of $\delta = 0.13(0.22)$ result in a more (less) cuspy DM distribution. The density normalization parameter ρ_{Ein} is set in terms of the local DM density, after including a contribution of the DD.

The profile of the DD component is assumed to be described by [34]

$$\rho_{DD}(R, z) = \rho_{0DD} \exp \left[\frac{1.68 (R_\odot - R)}{R_{1/2}} \right] \exp \left[-\frac{0.693 |z|}{z_{1/2}} \right], \quad (2)$$

where $R_{1/2}$ and $z_{1/2}$ are the half mass scale lengths in the Galactic plane and perpendicular to the Galactic plane, respectively, and $R_\odot = 8.5$ kpc. Here R is the cylindrical radial coordinate.

The ratio of the local DM density in the dark disk to the local DM density in the spherical halo ρ_{0DD}/ρ_{0sph} typically range between 0.2-1.5 [34], with the higher ratios being related to higher mass densities in the thick stellar disk rather than in the thin stellar disk. The thick stellar disk can be populated by thin stellar disk stars, if the thin stellar disk gets heated by very massive, high-redshift mergers. Another cause could be multiple pro-grate and low inclination mergers [34].

In the template analysis performed below we will restrict to the case:

$$\alpha/2 \equiv \rho_{0DD}/(\rho_{0sph} + \rho_{0DD}) \leq 0.5. \quad (3)$$

fixing [35, 36]:

$$\rho_{0sph} + \rho_{0DD} = 0.4 \text{ GeV cm}^{-3}. \quad (4)$$

Regarding the dark disc thickness, some authors [37] have suggested thicker disks, while thinner and less significant dark disks can also be the case; keeping in the parametrization of eq. 2 $R_{1/2} = 11.7$ fixed [34], we will test the half mass scale length values of $z_{1/2} = 0.5, 1.0, 1.5, 3.0$ kpc.

In the standard model for cosmology, cold DM structures form hierarchically, with small DM halos collapsing first and subsequently merging into larger and larger objects. Since tidal disruption may only be partially effective, massive DM halos, such as the halo of our own Galaxy, are expected to contain a vast population of subhalos, with mass spanning from a tiny seed mass up to a fraction of the hosting halo mass. The minimum mass is essentially associated to the free-streaming scale of DM particles, in turns depending on their temperature of kinetic decoupling in the early Universe; for WIMPs the minimum mass can be as small as about $m_{cut} = 10^{-6} M_\odot$ [38, 39], much lighter than the dwarf galaxy scale, possibly to the smallest environment which can host stellar populations and hence a luminous counterpart. Because of the highly non-linear nature of the merging process, up to now the only efficient technique to model in detail DM halos is the use of numerical N-body simulations; indeed large populations of substructures have been found in such studies. We will assume as primary reference in our analysis results from Via Lactea II (VLII)[40], one of the highest resolution simulations up to date of Milky Way-sized CDM halo (virial mass $M_h = 1.9 \times 10^{12} M_\odot$), with over one billion DM "particles" and nominal mass resolution of about $4100 M_\odot$ (numerical effects appear to enter well above this scale, possibly affecting the subhalo mass spectrum up to about $\sim 3 \times 10^6 M_\odot$). In our analysis we will discuss both the DM pair annihilation associated to individual DM substructures as well as the collective effect from the whole subhalo population; in both respects, the resolution of the simulations appears insufficient to properly model the expected signals. Our approach will then be to use the simulation results to properly calibrate the necessary extrapolations to smaller masses: tuning, at given Galactocentric radius, the subhalo pericenter distribution and applying a recipe for taking into account tidal stripping effects, we derive a model which reproduces fairly well the subhalo mass function and the distribution in halo concentration as a function of radius in the VLII simulation, and we use it as a prediction below its resolution (some details about our approach are given in Appendix A).

The general trends in the DM subhalo distribution can be understood from the fact that more massive objects are more prone to tidal stripping than the less massive ones, because they typically have smaller average density, reflecting the fact that they collapsed later in the cosmic history at a lower average background density. As the result, when going toward the center of the host halo, the average subhalo density increases and the average mass decreases. Also, in the inner part of a DM halo the tidal forces become stronger, possibly making the sub-

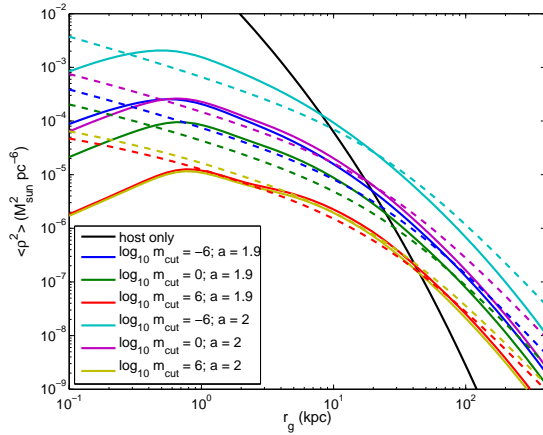


FIG. 1: Average DM squared density $\langle \rho^2 \rangle$ associated to subhalo population, as a function of Galactocentric radius r_g , for the case of a biased distribution (solid lines) and an anti-biased distribution (dashed lines), and for a few assumptions on the values for subhalo mass function a and minimum subhalo mass m_{cut} (see the text for details); also shown is the density squared of the smooth halo component.

halos spatial distribution to be anti-biased with respect to host density profile: this tendency has been found in some numerical simulations, see, e.g., [24, 41], while it has also been claimed that biased or anti-biased distributions may just stem from selection effects [23, 40]. The model in our extrapolation from the VLII results gives a biased distribution; to bracket uncertainties we consider also an anti-biased distribution which is instead taken from [24]. The other parameters entering most critically in our analysis are the spectral index a for the subhalo mass function and the minimum subhalo mass m_{cut} . In Fig. 1 we plot, as a function of Galactocentric radius, the average DM squared density associated to the full subhalo population, for two choices of the spectral index, i.e. $a = 1.9$ and $a = 2$, three sample values of the minimum subhalo mass, and for the biased (solid lines) and anti-biased (dashed lines) distributions; as a comparison the density squared of the smooth DM halo component, Eq. 1, with $\delta = 0.17$, is also given.

III. DM SUBSTRUCTURES IN THE MILKY WAY AND THE 2 γ -RAY LINES

In [19], 16 unassociated point sources have been identified with at least one 100-140 GeV photon for SOURCE event class. Among those photons, there are 9 photons in the ULTRACLEAN event class sample with energies ~ 111 and ~ 129 GeV. Those photons from unassociated point sources may imply a signal of DM annihilation in close by substructures. That ansatz can be compared with predictions from cosmological simulations.

The 2 yr point source catalogue [42] has 575 unassociated point sources. In [19], the 9 ULTRACLEAN

photons at $\simeq 111$ and 129 GeV lie within a $0.15^\circ/0.3^\circ$ radius for FRONT/BACK converted events covering an area of $0.07/0.28$ square degrees. Thus the 575 unassociated point sources cover at most $1.6 \times 10^2 \text{ deg}^2$ out of $4.1 \times 10^4 \text{ deg}^2$ and would give a conservative upper estimate of 5.06 photons out of the 1.3×10^3 [63]. The probability that 9 or more ULTRACLEAN class photons out of the 1.3×10^3 photons of the 4π sky fall within the area covered by the 575 unassociated point sources is $p = 0.0721$ [64]. Yet there may also be a bias toward discovering point sources around single high energy events [43]. While by itself not a strong statistical deviation, the coincidence in energy with the GC signal inclines us to test for alternative possibilities and whether some of these photons come from unassociated point sources that are DM subhalos.

The number of photons that we receive from a single subhalo with luminosity $L \equiv \int \rho_{\text{sub}}^2 dV$ and line of sight (los) distance λ from us, for channel $ch = \gamma\gamma$ or γZ is given by:

$$N_{\gamma}^{ch} = \mathcal{N}_{\gamma}^{ch} \frac{\langle \sigma_A v \rangle_{ch}}{2} \frac{L}{m_{\chi}^2} \frac{\tau_{\text{exp}} A_{\text{exp}}}{4\pi\lambda^2}, \quad (5)$$

where $m_{\chi} = 129 \text{ GeV}$ is the DM particle mass, and $\mathcal{N}_{\gamma}^{ch} = 1(2)$ for $\gamma Z (\gamma\gamma)$. τ_{exp} and A_{exp} are the detector's exposure time and effective area for photon's energy of 129 GeV, respectively. In this work, we use for the averaged *Fermi*-LAT exposure after $\simeq 4$ years $\tau_{\text{exp}} \times A_{\text{exp}} = 1.22 \times 10^{11} \text{ cm}^2 \text{ s}$. For this section, we consider two values of annihilation rates: $\langle \sigma v \rangle_{\gamma\gamma} = \langle \sigma v \rangle_{\gamma Z} = 0.98 \times 10^{-27} \text{ cm}^3 \text{ s}^{-1}$, a value derived assuming our default smooth component DM density profile (no DD) and fitting the monochromatic signal in the region $|l| < 5^\circ$ & $|b| < 5^\circ$ [17]; and $\langle \sigma v \rangle_{\gamma\gamma} = \langle \sigma v \rangle_{\gamma Z} = 3 \times 10^{-28} \text{ cm}^3 \text{ s}^{-1}$, which fits better the whole sky region (see section IV).

To quantify the possible impact of substructures in the line photons on the sky we ask the following questions:

- A) How many subhalos give 2 or more photons in to the 2 γ -ray lines?
- B) How many photons (in the two lines energies) do we get from all the subhalos that give a more than 0.1 photons?

The difference between the number of photons from the entire subhalo population received and the answer to question (B) is a proxy for the diffuse gamma-ray flux to the two lines from DM substructures gravitationally bound in the main DM halo. We will refer to these photons as "DM substructure diffuse".

In Table I we consider first the single subhalo sample from the VLII simulation [40] (no extrapolation below the mass resolution at this level) and compute answers to the questions formulated above, averaging over results obtained for 100 random choices for the position of the observer, all at fixed Galactocentric distance $R_{\odot} = 8.5 \text{ kpc}$ (the average is performed to wipe out fluctuations involving effects of nearby subhalos or voids in a single random choice). We then turn our analysis to the extrapolated subhalo populations focussing on the biased

Simulation Assump.	Q.A	Q.B
VLII	0 (0)	0.213 (0.024)
biased - case I	0.0198 (0.00344)	0.473 (0.0874)
biased - case II	0.0139 (0.0024)	0.342 (0.0618)
anti-biased - case I	0.0746 (0.0176)	1.24 (0.296)
anti-biased - case II	0.0898 (0.0196)	1.62 (0.361)

TABLE I: Relevance of substructures for detection of the monochromatic photons as referred to the questions A to B as posed in the text, using cross section which fits GC (fits the whole sky). Answers are provided in case of the subhalo sample from the VLII simulation itself and from extrapolations of it in case of biased or anti-biased distributions with the parameter choice $m_{cut} = 10^3 M_\odot$ & $a = 1.9$ (case I) and $m_{cut} = 10^{-6} M_\odot$ & $a = 2$ (case II). Changing the overall normalization of the subhalo number density would shift the results provided in the table accordingly, e.g., by a factor of about 2 if adopting the normalization of the Aquarius simulation [41].

and anti-biased distribution and considering two possible extrapolations for lowest subhalo mass and subhalo mass spectral index, bracketing extreme possibilities, case I corresponding to $(m_{cut}, a) = (10^3 M_\odot, 1.9)$ and case II to $(m_{cut}, a) = (10^{-6} M_\odot, 2)$. The number of line photons received is computed including only subhalos within the virial radius since we find that for VLII subhalos only 0.5% of the total photon comes from substructures lying outside it. On the other hand there is a further uncertainty one should be careful about: by tuning our subhalo model to the VLII results we are fixing the normalization of subhalo number density (above mass resolution) for the Milky Way halo according to that specific realization; this is a quantity which actually has a certain scattering among different halo realizations and different simulations, e.g., referring to the results of the Aquarius simulation [41] we should increase such normalizing of about a factor of 2, shifting results in Table I by the same factor.

As a further test, in Table II we report the total number of monochromatic photons expected from our entire subhalo populations under a set of different assumptions for spectral index and cutoff mass. The results are again shown for biased and anti-biased distributions.

If the photons from unassociated point sources are from DM annihilation in substructures, their number (9 ULTRACLEAN events) probes the number of photons from the brighter substructure subsample. Considering that the number of photons originating from subhalos that emit more than 0.1 photons in the two lines (i.e. the results of Question B in Table I), is indicative of such number of photons, we compare the probability of having observed 9 (or more) photons for a DM signal calculated in the VLII sample (0.213 photons), in extrapolation for biased distribution and case I (0.473 photons), for anti-biased distribution and case I (1.24 photons), for biased distribution and case II (0.342 photons), and for anti-biased distribution and case II (1.62 pho-

tions). These probabilities are $p = 0.0874$ for the background plus the DM signal stemming from VLII sample, $p = 0.108(0.185)$ for background plus the DM signal in the extrapolation for biased (anti-biased) distribution in case I and $p = 0.0975(0.23)$ for background plus the DM signal in the extrapolation for biased (anti-biased) distribution in case II. Using the normalization from Aquarius simulation would increase the number of subhalos and received photons by a factor of 2, shifting the probabilities to, respectively, $p = 0.153(0.344)$ and $p = 0.127(0.449)$. Thus the most conservative VLII assumptions case is marginally favorable than the just background case. When extrapolating below the mass resolution, probabilities increase further, reaching relevant levels in optimistic extrapolations. On the other hand, using the cross section which fits the whole sky (see section IV), we don't see much differences in the p-values from having just a background signal. Also, from Question A, there are no subhalos expected to give more than 2 photons. One must keep in mind that lowering the value of cross section by a factor of 3, by going from σv which fits GC better to the one which fits the whole sky better, does not simply reduce all the values in Table I by the same factor. This is because the photons produced by each subhalo will decrease; so that some subhalos which previously gave more than, say, 0.1 photons; will now give less. The photons coming from such subhalos are not included anymore. (Similarly with the numbers of subhalos which give more than 2 photons.) However, in Table II, all values do lower by the same factor, because they are the number of photons coming from all subhalos.

The differences between the numbers of photons that originate from all DM subhalos (Table II) and the numbers of photons that originate from DM subhalos that contribute 10^{-1} lines photons or more (Q.B) are conservative probes to the diffuse contribution from the DM subhalos at $\simeq 111$ and 129 GeV. The VLII sample gives $1.21 - 0.213 = 1.0$ DM substructure diffuse component photon, extrapolation for the biased (anti-biased) distribution in the case I $5.46 - 0.473 = 4.99$ ($3.9 - 1.24 = 2.66$) photons, while in case II $96 - 0.342 = 95.7$ ($87 - 1.62 = 85.4$) photons. An upper (rough) limit to the DM substructure diffuse $\simeq 111$ and 129 GeV photon component can be derived by considering it approximately isotropic and then counting the $\simeq 111$ and 129 GeV photons laying above $|b| \geq 60^\circ$ times 7.46 (the ratio of 4π to the area of the sky with $|b| \geq 60^\circ$). There are 40 ± 5 GeV and 30 ± 6 GeV photons above $|b| \geq 60^\circ$, i.e. an upper estimate of the $\simeq 111$ and 129 GeV photons in the isotropic component is 522 photons; thus significantly larger than the 1.0, 4.99 (2.66), or 95.7 (85.4) DM substructure diffuse component photons predictions from VLII and biased (anti-biased) case I and II. In section IV we have a more model-dependent estimate of the isotropic 111 and 129 GeV γ -rays component, which though decreases the isotropic component photons down to $\simeq 190$ -230.

While for the anti-biased distribution we find more

Index "a"	m _{cut} (M _⊙)	biased	anti-biased
2.0	1.0×10 ⁻⁶	96	87
2.0	1.0	20.8	20.4
1.9	1.0×10 ⁻⁶	16.3	10.2
1.9	1.0×10 ³	5.46	3.90
1.9	2.0×10 ⁴	4.02	2.99

TABLE II: Number of 111 and 129 GeV lines photons contributing to the DM subhalo diffuse lines component, for various choices of subhalo distributions, using cross section which fits GC (using cross section which fits whole sky instead, will scale all values by a factor of $\simeq 3/9.8 = 0.3$). We show results for different subhalo mass function spectral index a and lower mass cut-off m_{cut} , and for biased and anti-biased distributions.

events from fewer sources than the biased distribution, since the subhalo concentration has a sharper dependence on Galactocentric radius with higher luminous subhalos closer to the GC, here the trend is reversed when summing over the whole population of dim sources.

IV. DIFFUSE γ -RAY LINES EMISSION FROM DARK MATTER ANNIHILATION

As discussed in II the γ -ray lines centered at 111 and 129 GeV that are observed in the sky originate from combination of sources. We mask out the contribution from the 16 point sources detected at [19] with one photon at energies between 100-140 GeV. We also mask out the extended sources (galaxy clusters) where a similar excess of 100-140 GeV γ -rays has been observed [18]. We use a mask of 0.5° in radius for each of the 16 the point sources of [19] and a 4° radius mask for the targets of [18]. The remaining contribution to the 111 and the 129 GeV lines may come from the diffuse γ -rays emission due to DM annihilations in the main halo and its dark disk, from background γ -rays produced in the Milky Way, from DM annihilation at small scale substructures in the Milky Way (that we have not yet identified as point sources) and from other isotropically distributed extragalactic astrophysical sources. DM annihilation in extragalactic structures and CR contamination will give an additional isotropic component. In Fig. 2 we show the 4π sky after implementing our mask on the 16 point sources and the 6 extended ones.

The DM annihilation rate in any part of the Galaxy is given by:

$$\Gamma_{ann} = \frac{1}{2m_\chi^2} \langle \sigma_{ann} | v \rangle \quad (6)$$

$$\times (\rho_{sph}^2 + \rho_{DD}^2 + 2\rho_{sph} \cdot \rho_{DD} + \rho_{sub}^2),$$

with $\langle \sigma_{ann} | v \rangle$ the annihilation cross-section taken to be the same for both the DM particles in the dark disk, the spherical halo and the substructures. For the case of Sommerfeld enhancement these cross-sections are in gen-

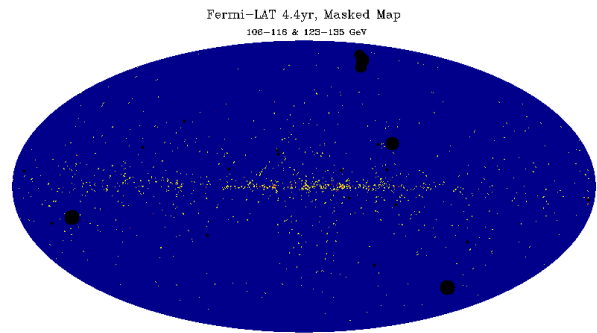


FIG. 2: γ -ray events (ULTRACLEAN class) with energy of 111 ± 5 and 129 ± 6 GeV after 4 yrs of collection by *Fermi*-LAT. We mask out the 16 point sources of [19] and the 6 extended sources of [18] (see text for more details). We present γ -ray events in Mollweide projection using HEALPix [44].

eral different, because of the dependence of the annihilation cross-section to the velocity dispersion of dark matter [45–48] and the fact that for the DM particles in the DD the dispersion is suppressed by a factor of 5-6 compared to that in the spherical halo components [34]; with subhalos having even lower velocity dispersions. Thus for Sommerfeld enhanced models the dark disk contribution to CRs and γ -rays can be much more significant [49] (see also [50] for a discussion on the impact of subhalos).

In fitting to the 2 γ -ray line full sky data we probe the prompt γ -ray DM annihilation component of the spectrum which is directly related to the annihilation rate in eq. 6.

We use the masked full sky data with energies 111 ± 5 GeV and 129 ± 6 GeV. We perform a maximum likelihood fit calculating the log-likelihood based on [51]:

$$\ln \mathcal{L} = \sum_i k_i \ln \mu_i - \mu_i - \ln(k_i!), \quad (7)$$

where μ_i is the model of linear combination of templates at pixel i , and k is the map of observed counts which is just the single 111 ± 5 GeV and 129 ± 6 GeV γ -ray *Fermi* masked map. Our *diffuse* γ -ray model is composed of 6 templates with 4 free parameters:

$$\begin{aligned} \mu_i = & N \cdot \text{Back}_i + A \cdot [(2 - \alpha)^2 \cdot \text{SphDM}_i \\ & + \alpha^2 \cdot \text{DarkDisk}_i + \alpha(2 - \alpha) \cdot \text{MixedDM}_i \\ & + \text{SubDM}_i] + B \cdot \text{Iso}_i. \end{aligned} \quad (8)$$

The Back_i template comes from our DRAGON run and is kept fixed modulo a normalization N for a specific set of assumptions on the ISM and ISRF, the SphDM_i refers to the term in eq. 6 that is proportional to ρ_{sph}^2 . The DarkDisk_i template refers to the term in eq. 6 proportional to ρ_{DD}^2 and the MixedDM_i template to the $2\rho_{sph} \cdot \rho_{DD}$ term. The contribution of dim Galactic DM subhalos to the diffuse γ -rays is included in the "SubDM" (related to the ρ_{sub}^2 term in eq. 6), where as described earlier we have masked out the brightest possibly detected

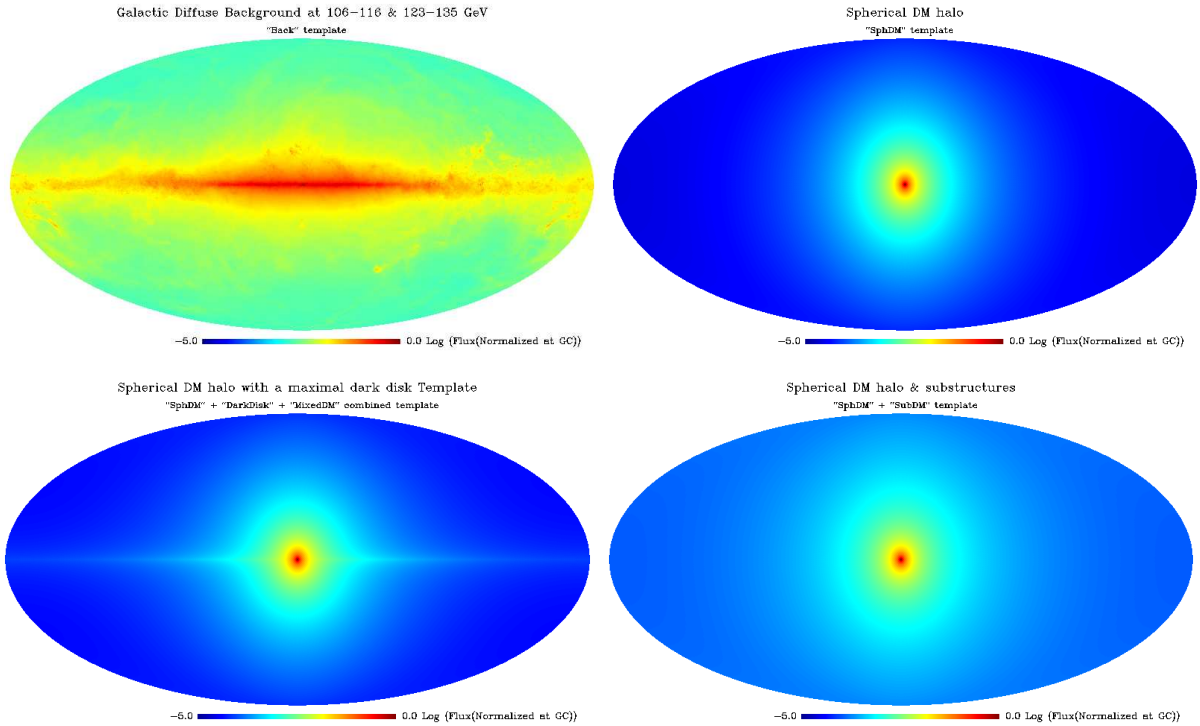


FIG. 3: The γ -ray templates as can be used in eq. 8. *Top left*: the Galactic diffuse background template including the π^0 , inverse Compton scattering and bremsstrahlung components at energies of 111 ± 5 and 129 ± 6 GeV. We show the "Back A" model. *Top right*: the diffuse DM spherical halo component assuming an Einasto with $\delta = 0.13$ profile. *Bottom left*: diffuse emission from the combined spherical and dark disk DM distributions, assuming a maximal dark disk ($\alpha = 1$), which results in showing the "SphDM" + "DarkDisk" + "MixedDM" combined template. We use Einasto profile with $\delta = 0.13$ for the spherical and $z_{1/2} = 0.5$ kpc for the scale height of the dark disk. *Bottom right*: the DM diffuse subhalo template "SubDM" for biased distribution with $m_{cut} = 10^{-6} M_\odot$ together with the spherical DM halo "SphDM" template (Einasto with $\delta = 0.13$). We use Mollweide projection. To demonstrate the different morphologies, each template is normalized to 1 at the GC. Dark blue (dark grey) color refers to a flux suppressed by a factor of 10^{-5} compared to the GC in each template. In eq. 8 we use the calculated flux values from the DRAGON package.

members. α refers to the ratio of local DM density of the DD over the spherical halo given in eq. 3. The Iso_i template includes the contribution of DM extragalactic annihilations, the extragalactic background from other sources and the possible CR contamination. We also multiply the model map by the total FRONT+BACK-converted ULTRACLEAN photons exposure map and multiply by the mask. In Figure 3 for specific choices we show 4 different templates. On top left a specific model ("Back A") for the Galactic diffuse background is shown at the energies of interest. On top right we plot the "SphDM" template for an Einasto DM spherical halo profile with $\delta = 0.13$, and on bottom left we show the combined DM spherical and dark disk for $\alpha = 1$ ("SphDM" + "DarkDisk" + "MixedDM"). The DM subhalos contribution ("SubDM") is given in the bottom right. We use HEALPix [44] with $N_{side} = 128$ which represents closer the angular resolution of *Fermi* LAT at these energies [65].

We also calculate the significance of a DM contribution from the diffuse by the test statistic, where

$$TS \equiv -2 \ln \frac{\mathcal{L}_{null}}{\mathcal{L}_{best fit}}. \quad (9)$$

$\mathcal{L}_{best fit}$ allows for the DM to contribute, while in \mathcal{L}_{null} we set the DM diffuse component to zero and refit the other two diffuse components. Our results are shown in Tables III-V.

Ignoring first both the contribution of a dark disk and the DM subhalos, we find that the more cuspy DM profiles for the main/spherical halo that lead to less DM contribution to the diffuse γ -ray spectrum away from the Galactic center, provide a larger positive fit to the 4π sky (see Table III). Yet the significance of that is not very large ($TS = 9.1/9.2$ and 11.9 in the best cases). An even more cored (flat) Burkert DM profile for the main halo in the inner kpcs does not give a better fit to the 111 and 129 GeV lines distribution in agreement with the findings of [2] and [1] performed in subsections of the sky.

Using the model of $\delta = 0.13$ for the Einasto DM density profile that provides the best fit, we also test differ-

DM profiles / Backgrounds	σv	F_{iso}	Back ph.	DM ph.	Iso ph.	TS
Ein. ($\delta = 0.13$) / Back A	1.5 (4.5)	5.73	1146	40 (121)	214	9.1
Ein. ($\delta = 0.17$) / Back A	2.2 (7.1)	5.55	1146	43 (138)	207	6.1
Ein. ($\delta = 0.22$) / Back A	2.7 (8.5)	5.38	1157	41 (127)	201	2.8
Ein. ($\delta = 0.13$) / Back B	1.6 (4.8)	5.87	1134	44 (129)	219	11.9
Ein. ($\delta = 0.13$) / Back C	1.5 (4.6)	5.81	1144	39 (124)	217	9.2
Ein. ($\delta = 0.13$) / Back D	1.3 (4.3)	6.05	1137	36 (115)	226	7.8

TABLE III: The values of relevant parameters for various assumptions on the Galactic diffuse background and the distribution of DM spherical halo ignoring the contribution of DD ($\alpha = 0$) and subhalos. Second column gives the best fit annihilation cross-section assuming equal annihilation cross-sections to the two lines; $\langle\sigma v\rangle_{\gamma Z} = \langle\sigma v\rangle_{\gamma\gamma} \equiv \sigma v$ in units of $\times 10^{-28} \text{ cm}^3 \text{ s}^{-1}$. F_{iso} is the calculated isotropic flux at 111 ± 5 GeV and 129 ± 6 GeV in units of $\times 10^{-12} \text{ GeV}^{-1} \text{ cm}^{-2} \text{ s}^{-1} \text{ sr}^{-1}$. Columns 4-6 refer to the 111 ± 5 GeV and 129 ± 6 GeV photons in the Background, DM and Isotropic diffuse components as predicted by the fitted values of N , A and B of eq. 8. Last column gives the TS for detection of DM signal. Values in parentheses refer to 3σ upper limits on the DM annihilation cross-section.

DM profiles / Backgrounds	σv	F_{iso}	Back ph.	DM ph.	Iso ph.	TS
Ein. ($\delta = 0.13$); DD $z_{1/2} = 0.5$ / Back A	2.8	5.72	1143	43	213	8.7
Ein. ($\delta = 0.13$); DD $z_{1/2} = 1.0$ / Back A	2.6	5.69	1144	42	212	8.0
Ein. ($\delta = 0.13$); DD $z_{1/2} = 1.5$ / Back A	2.5	5.64	1146	43	210	7.7
Ein. ($\delta = 0.13$); DD $z_{1/2} = 3.0$ / Back A	2.4	5.60	1145	45	209	7.6
Ein. ($\delta = 0.17$); DD $z_{1/2} = 0.5$ / Back A	4.2	5.56	1143	49	208	5.6
Ein. ($\delta = 0.22$); DD $z_{1/2} = 0.5$ / Back A	4.7	5.40	1154	43	201	2.4
Ein. ($\delta = 0.13$); DD $z_{1/2} = 0.5$ / Back B	3.1	5.91	1130	48	221	11.5
Ein. ($\delta = 0.13$); DD $z_{1/2} = 0.5$ / Back C	2.8	5.79	1141	43	216	9.0
Ein. ($\delta = 0.13$); DD $z_{1/2} = 0.5$ / Back D	2.5	6.04	1135	38	225	7.5

TABLE IV: The values of relevant parameters for various assumptions on the Galactic diffuse background, the distribution of DM spherical halo and the DD assuming the maximal DD contribution ($\alpha = 1$) and ignoring the contribution of subhalos. Second column is as in Table III, F_{iso} is in units of $\times 10^{-12} \text{ GeV}^{-1} \text{ cm}^{-2} \text{ s}^{-1} \text{ sr}^{-1}$ and σv is in units of $\times 10^{-28} \text{ cm}^3 \text{ s}^{-1}$. Columns 4-6 refer to the 111 ± 5 GeV and 129 ± 6 GeV photons in Back, DM and Iso components predicted by the fitted values of N , A and B . Last column gives the TS for detection of DM signal.

ent diffuse background models ("Back A"-"Back D") to account for uncertainties in the interstellar medium gas distribution and interstellar radiation field distribution. We find that in all cases a DM component is preferred by the fit at $\simeq 2$ - 3σ significance for the cuspy DM models (1-sided since in our fits we allow for the DM component to be even negative), and accounting for about 35-45 photons (cross-sections of $\langle\sigma v\rangle = 1.3 - 2.7 \times 10^{-28} \text{ cm}^3 \text{ s}^{-1}$) [66]. As with "Back A" the cuspy DM profiles are preferred for the tested backgrounds. Our "Back A" is the same as the reference model described in [29], which was shown to provide a good agreement to the 4π sky and in energies between 1 and 200 GeV and has also been cross-checked to local CR measurements. Model "Back B" assumes a different distribution for the molecular hydrogen gas component that is dominant at lower latitudes and toward the GC where many of the 111 and 129 GeV photon excess have been claimed (see [29] for more details). "Back C" and "Back D" Galactic diffuse models assume, respectively, an enhanced ISRF energy density distribution toward the disk and a minimal metallicity gradient [52]. The latter assumption affects both the morphology and the spectrum of the ISRF and as a result the γ -rays produced via Compton up-scattering of these photons by high energy CR electrons. These background models are discussed in further detail in [29]. They have not been

constructed to study just the Galactic γ -ray background at ~ 110 -130 GeV, but instead the general uncertainties in the Galactic diffuse γ -rays between 1-200 GeV, in the full sky and in subsections of it.

Since in our fits we also allow for an isotropic component we can calculate the isotropic flux at these energy ranges, taking into account also the Galactic diffuse background uncertainties. We find that $\simeq 210 - 230$ photons can be accounted by that component. This gives an isotropic flux of 5.6 - $6.1 \times 10^{-12} \text{ GeV}^{-1} \text{ cm}^{-2} \text{ s}^{-1} \text{ sr}^{-1}$ which is in agreement with the extragalactic isotropic γ -ray flux of [53] described by $dN/dE \propto E^{-2.41 \pm 0.05}$ measured between 200 MeV and 100 GeV. The $\simeq 210 - 230$ photons of the isotropic component can also be used to set approximate limits on the contribution from DM halos at extragalactic distances.

We find that adding a dark disk component does not significantly change the fit to the data from the case of having only a spherical DM halo contribution. That is for any choice of diffuse background or spherical DM halo shown Table IV. Thus a significant DD contribution is not preferred by the current data; while yet it can not be excluded either. We give the likelihood fits for the maximal DD contribution.

DM profiles	σv	α	F_{iso}	Back ph.	DM ph.	Iso ph.	TS
Ein. ($\delta = 0.13$); Biased Sub. Dist. ($m_{cut} = 10^{-6} M_{\odot}$)	1.4	0.0	5.34	1146	53(16)	199	8.6
Ein. ($\delta = 0.13$); Biased Sub. Dist. ($m_{cut} = 10^{+6} M_{\odot}$)	1.5	0.0	5.70	1146	40(0.36)	213	9.1
Ein. ($\delta = 0.13$); Anti-Biased Sub. Dist. ($m_{cut} = 10^{-6} M_{\odot}$)	1.4	0.0	5.39	1146	52(14)	201	8.8
Ein. ($\delta = 0.13$); Anti-Biased Sub. Dist. ($m_{cut} = 10^{+6} M_{\odot}$)	1.5	0.0	5.70	1146	40(0.41)	213	9.1
Ein. ($\delta = 0.17$); Biased Sub. Dist. ($m_{cut} = 10^{-6} M_{\odot}$)	2.0	0.0	5.07	1149	61(23)	189	5.2
Ein. ($\delta = 0.17$); Biased Sub. Dist. ($m_{cut} = 10^{+6} M_{\odot}$)	2.4	0.0	5.54	1146	46(0.59)	207	6.1
Ein. ($\delta = 0.17$); Anti-Biased Sub. Dist. ($m_{cut} = 10^{-6} M_{\odot}$)	2.1	0.0	5.10	1149	60(21)	190	5.5
Ein. ($\delta = 0.17$); Anti-Biased Sub. Dist. ($m_{cut} = 10^{+6} M_{\odot}$)	2.4	0.0	5.54	1146	47(0.66)	207	6.1
Ein. ($\delta = 0.13$); DD $z_{1/2} = 0.5$; Biased Sub. Dist. ($m_{cut} = 10^{-6} M_{\odot}$)	2.4	1	5.04	1144	64(28)	188	7.8
Ein. ($\delta = 0.13$); DD $z_{1/2} = 0.5$; Biased Sub. Dist. ($m_{cut} = 10^{+6} M_{\odot}$)	2.8	1	5.769	1143	43(0.69)	212	8.7
Ein. ($\delta = 0.13$); DD $z_{1/2} = 0.5$; Anti-Biased Sub. Dist. ($m_{cut} = 10^{-6} M_{\odot}$)	2.6	1	5.13	1143	64(25)	192	8.2
Ein. ($\delta = 0.13$); DD $z_{1/2} = 0.5$; Anti-Biased Sub. Dist. ($m_{cut} = 10^{+6} M_{\odot}$)	2.8	1	5.69	1143	43(0.77)	212	8.7

TABLE V: The values of relevant parameters for various assumptions on the distribution of DM spherical halo, the DD and dim Galactic DM subhalos with different choices of the minimal subhalo mass. Units for σv and F_{iso} are as in Tables III and IV. In parentheses we give the photon number associated to the subhalo diffuse component only. The subhalo mass spectral index is assumed to be -2. In all cases we use our reference "BackA" as Galactic diffuse background.

Our fits give a relatively flat behavior in the parameter α with a slight preference for $\alpha \rightarrow 0$. More specifically for a DD with $z_{1/2} \geq 1.5$ kpc (thick DD) with $\alpha \rightarrow 1$ we get a lower test statistic by about $\Delta TS \simeq 2$ compared to the cases of having only the spherical DM halos contributing, i.e. the data show a slight preference for having only a spherical DM halo at these energies. That is for any of our background assumptions. Yet thin DD ($z_{1/2} \simeq 0.5$ kpc) give about the same TS as the only spherical DM halo contribution for any of our background models. Having tested also the 4 yr sample, that gave a slight preference for $\alpha = 1$ with a $z_{1/2} \simeq 0.5$ kpc DD we conclude that the current small number of photons at the two energy lines does not provide us with enough detail to discriminate a thin DD component from the disk-like distribution of the Galactic background γ -rays. With more γ -ray data we expect that we will be able to further disentangle the different γ -ray morphologies.

Even for the case where we have a maximal DD contribution, i.e. when $\alpha = 1$ most of the DM photons are due to the spherical and the mixed terms of eq. 6. In those cases, the equivalent DM annihilation cross-section that accounts for the DM template normalization is maximal. That is the case since the total number of DM photons is about the same while the $(\rho_{sph}^2 + \rho_{DD}^2 + 2\rho_{sph} \cdot \rho_{DD})$ term in eq. 6 is minimal. Since the DD term can not be excluded this is a way of allowing for higher annihilation cross-sections, by up to a factor of $\simeq 2$.

In Table V we also study the impact of the diffuse DM subhalo template "SubDM" of eq. 8 with and without a DD component. To bracket the uncertainties we used both the biased and the anti-biased Galactic subhalo distributions (see Appendix). We also tested the subhalo mass extrapolations down to $10^{+6} M_{\odot}$ and $10^{-6} M_{\odot}$. For the cases where the extrapolation is down to $10^{+6} M_{\odot}$ the DM subhalo diffuse component is subdominant contributing only a few line photons. On the contrary, for extrapolations down to $10^{-6} M_{\odot}$ that component can con-

tribute up to $\sim 1/3$ ($\sim 1/2$) of the Galactic DM line photons, with the remaining coming from the spherical main halo (spherical & DD components). With the current data the difference in the TS fit between the biased and the anti-biased distributions is very small (see Table V). Yet, even adding a strong subhalo term/template, our method can discriminate between different assumptions for the cuspieness of the spherical halo "SphDM". In agreement with all our previously discussed tests, a preference toward cuspiest halos is found. In Table V we compare between $\delta = 0.13$ and $\delta = 0.17$ Einasto profiles that differ only in the inner few degrees from the GC.

Having tested the DM case both with and without a dark disk and including/excluding the contribution of Galactic bound dim DM subhalos we have consistently found a thermally averaged cross-section $\langle \sigma v \rangle \equiv \langle \sigma v \rangle_{\gamma\gamma} = \langle \sigma v \rangle_{\gamma Z}$ for the two lines that is in the range of $1.5\text{--}4.5 \times 10^{-28} \text{ cm}^3 \text{s}^{-1}$. These values are a factor of 9-3 smaller than the suggested values from analyses coming when concentrating only toward the GC [1]. Fitting the entire 4π sky can dilute the DM signal from the GC and thus suggest a smaller annihilation cross-section. Yet, we note that a strong annihilation cross-section to the lines should be seen at the diffuse spectrum at high latitudes when including the contribution from the dim subhalos with masses down to the free streaming scale. Our fits do not suggest such a case. Taking the subhalos to have masses down to $10^{-6} M_{\odot}$, we get from our fits shown in Table V $\simeq 15\text{--}20$ photons (30 including a DD in the fit) from annihilations just in the dim subhalos. That number of photons from the diffuse subhalo component can be explained by a thermally averaged cross-section of $1.5\text{--}2.5 \times 10^{-28} \text{ cm}^3 \text{s}^{-1}$. Given that the velocity dispersion in bound substructures is smaller than in the GC or locally that may be expected. Alternatively explained, thermally averaged cross-section of $\langle \sigma v \rangle = 1.0 \times 10^{-27} \text{ cm}^3 \text{s}^{-1}$ down to the smallest subhalos would give ~ 100 photons on the 4π sky just on the two lines and just from the dim Galactic subhalos. Of these $\simeq 25$ photons would

be at $|b| \geq 45^\circ$ with the isotropic component predicting $\simeq 70$ photons in the two energy ranges (111 ± 5 , 129 ± 6 GeV). Thus the lines would have to be observed at high latitudes as well. If not found at these latitudes, then either the $\langle\sigma v\rangle$ is smaller in the subhalos, in general, or subhalos are not formed down to masses of $\sim 10^{-6}M_\odot$. We note that in the above numbers we have not included the possible and more model dependent contribution from extragalactic DM annihilations.

V. DISCUSSION AND CONCLUSIONS

Recently, [19] has found indications for the 111 and the 129 GeV lines in the 2 yr *Fermi* unassociated point sources catalogue that would be indicative for DM annihilation in substructures. We compare the compatibility of the findings of [19] with the results from VLII cosmological simulations and extrapolations of it. In that process we have assumed the same annihilation cross-section to the Galactic center lines signal [1–6] given that the point sources lines signal and the Galactic center line(s) signal have been observed at the same γ -ray energies. We find that just considering VLII assumptions we do not get enough line photons from the brightest Galactic DM subhalos to claim agreement with the signal seen by [19]. Yet completions of the VLII simulation results do give a number of line photons from the brightest subhalos that in the most optimistic cases is in good agreement with (but still below) the lines events number found by [19] (9 events in their ULTRACLEAN sample) (see discussion in section III). These most optimistic extrapolations to very small substructures ($10^{-6}M_\odot$) do not predict that many diffuse line photons to be conservatively constrained by the γ -ray flux at high latitudes. The same applies when we compare their predictions to the isotropic γ -ray flux which for the energies of the lines we have calculated to be centered at $5.6 \pm 0.3 \times 10^{-12} \text{ GeV}^{-1} \text{ cm}^{-2} \text{ s}^{-1} \text{ sr}^{-1}$, with 4π sky fit values being in the range of $5.0 - 6.0 \times 10^{-12} \text{ GeV}^{-1} \text{ cm}^{-2} \text{ s}^{-1} \text{ sr}^{-1}$ (accounting for systematic uncertainties in the evaluation of the isotropic component).

Most of the 111 and the 129 GeV line photons on the γ -ray sky are not from DM annihilations but rather from the Galactic diffuse and the isotropic diffuse background (shown in Fig. 2). By doing a template fit to the 4π sky, we test how robust the DM signal hypothesis is for different physical assumptions on the Galactic diffuse γ -ray background flux and on the DM halo profile (see discussion on section IV). We find a positive fit of having a DM spherical halo component. Our DM annihilation component hypothesis is preferred to the case without a DM component at a test statistic significance of up to 12; with the values depending on the exact DM halo assumptions. More concentrated DM profiles give a larger significance to a DM signal. We also find that our results on the positive signal of DM annihilation are weakly dependent on Galactic diffuse background uncertainties related to either the uncertainties in the distribution of the

interstellar medium gas or to the energy density in the interstellar radiation field.

Extending our set of tests on the DM distribution in the Galaxy, we include a dark disk component that could explain the non-isotropic distribution on the sky of the point sources of [19]. Our fits can not strongly favor or disfavor a significant disk-like DM component, even though there is a small preference toward thinner dark disks. We also study the contribution of the dimmest DM subhalos in the Milky Way to the diffuse gamma-ray sky at energies around 111 and 129 GeV and find a preference toward an anti-biased distribution of the subhalos within the main spherical DM halo. Yet our analysis is somewhat constrained in its power by the small number of photons on the sky at the energies of the 2 lines. As more statistics are being accumulated, a better understanding of the morphology of the γ -ray sky will be achieved allowing for such a template analysis to further disentangle the background γ -ray sky from any possible DM component.

Finally using the various combinations of backgrounds and DM distributions, we find the thermally averaged annihilation cross-section to be smaller than what has been originally suggested, with values ranging between $1.5 - 4.5 \times 10^{-28} \text{ cm}^3\text{s}^{-1}$. While the full sky fits are not optimal for a DM signal toward the GC, they include high latitudes which probe also the contribution from smaller substructures. A suppressed flux at high latitudes to the lines either indicates a smaller overall cross-section or a suppressed contribution from smaller substructures compared to the GC.

Acknowledgments

The authors would like to thank Alex Drlica-Wagner, Carmelo Evoli, Andrew Hearin, Dan Hooper, Ran Lu, Meng Su and Gabriella Zaharijas for valuable discussions. PU acknowledges partial support from the European Union FP7 ITN INVISIBLES (Marie Curie Actions, PITN-GA-2011-289442). In this work the authors have used the publicly available *Fermi*-LAT data and Fermi Tools archived at <http://fermi.gsfc.nasa.gov/ssc/>. We also acknowledge the use HEALPix.

Appendix A: DM Signal from Biased and Anti-Biased Distributions of Subhalos in the Milky Way

We fit the subhalos in the VLII simulation [40, 54] with NFW profile [24]:

$$\rho_{sub}(r) = \rho_s \left(\frac{r}{r_s} \right)^{-1} \left(1 + \frac{r}{r_s} \right)^{-2}. \quad (\text{A1})$$

and reading out the scale radius, r_s , and scale density, ρ_s , in terms of the peak of circular velocity V_{max} and the

corresponding radius r_{Vmax} (see, e.g. equation 9-10 in [24]), and their luminosities as:

$$L = 4/3\pi r_s^3 \rho_s^2 \left[1 - (1 + r_t/r_s)^{-3} \right], \quad (\text{A2})$$

where r_t is their tidal radius. By using this formula, combined with eq. (5), we find the results in the first row of Table I.

In deriving the biased distribution of subhalos, first, we calculate the gravitational potential from the host halo, cutting the profile at its virial radius, and distinguish bound subhalos from the unbound ones. There are 13510 bound subhalos, 9372 of them are within virial radius. We also calculate each subhalo's pericenter, r_p , to obtain the pericenter probability distribution function (PDF) as a function of Galactocentric radius, r_g , e.g. $dP/dr_p(r_p, r_g)$. For *unbound subhalos*, we identify their tidal radius as their *virial radius*, and their tidal mass as their *virial mass*. According to virial theorem, the average density inside virial radius should be the same for all halos. We find that this is indeed the case in VLII simulation: the average density inside virial radius of unbound subhalos is $\Delta_0 \rho_{crit}$, where Δ_0 is the overdensity relative to critical matter density for spherical collapse for $z = 0$, and ρ_{crit} is the critical *matter* density. For bound subhalos, tidal radius is usually much smaller than virial radius because of tidal stripping. We define the tidal concentration of a subhalo, c_t , as its average density within tidal radius divided by critical matter density; for unbound subhalos, $c_t = \Delta_0$. To determine the virial concentration PDF for unbound subhalos, we use the Bullock model [55] as parametrized in eq. (2) of [56] which relates the median virial concentration of a subhalo, $c_{vir} = r_{vir}/r_s$, with its virial mass, m_{vir} . We find that this parametrization can fit *unbound subhalos's* virial concentrations fairly well. We take the mass PDF of *unbound* subhalos to be a power law, $dP/dm_t \propto m_t^{-a} \Theta(m_t - m_{cut})$, and vary the spectral index $a = [1.9, 2]$. In fitting the mass and concentration PDF, we use the unbound subhalos because they are not tidally stripped. Hence, in this model, the Galactocentric radial dependence of mass and concentration will appear later, after they are tidally stripped by their host. To find subhalo's minimum concentration at some Galactocentric radius r_g , we apply the Roche criteria: for a subhalo in circular orbit, subhalo's self-gravity at r_t should be equal to the differential gravity pull of the host halo computed at r_g . As the subhalo's orbit is not exactly circular, the tidal force is strongest at its pericenter, so the concentration is determined by the tidal forces at its pericenter [57]:

$$c_{tr}(r_p) = \frac{2\overline{\rho_h}(< r_p)}{\rho_{crit}} - \frac{3\rho_h(r_p)}{\rho_{crit}}, \quad (\text{A3})$$

where ρ_h is VLII host density profile. We then refine the previous estimate by taking into account the pericenter radius distribution for subhalos, dP/dr_p . Subhalos initially with $c_t = \Delta_0 > c_{tr}(r_p)$ are left intact, whereas

subhalos initially with $c_t < c_{tr}(r_p)$ are tidally stripped until $c_{tr}(r_p)$ is reached, e.g.:

$$c'_t = \max[c_{tr}(r_p), \Delta_0]. \quad (\text{A4})$$

It is a fair approximation that scale ρ_s and r_s do not change in this process [58]. By following these steps; a subhalo's mass, concentration, and luminosity after tidal stripping are completely determined by its pericenter, mass, and concentration before tidal stripping. We then calculate the average mass, concentration, and luminosity after tidal stripping, and compare them against simulation. We find that luminosity and mass can be fitted very well, with best fit parameters $(m_{cut}, a) = (10^{6.5}, 1.9)$. (The m_{cut} here is the minimum subhalo mass *before* tidal stripping.) Our model also fits the tidal concentration very well near host center, although slightly deviates near its virial radius. This might indicate that our treatment of dynamical effects is oversimplified. Especially, the minimum concentration calculated by Roche criteria is only achieved after several pericentric passages [58–60], whereas in our model, we assume that all of them are already above minimum concentration. However, the procedure is validated by very good fits to the luminosities. Besides, it is conceptually simple and can be easily generalized to other host and subhalo mass profiles, and redshifts.

Regarding the subhalos number density profile, we consider both biased and anti-biased case. As mentioned in the section III, the strong tidal force near GC could make the subhalos spatial distribution to be anti-biased with respect to the host density profile. Indeed, for VLII itself, we find that the deviation from biased starts to happen around ~ 30 kpc. However, we find that the subhalo spatial distribution for VLII is more biased with respect to VLI [22, 54], which has lower resolution. This might indicate that the anti-biased is the result of numerical effect (The strong tidal force could strip subhalos until they are below or near resolution limit, hence undetectable as subhalos.) Also, VLII subhalos which are selected by mass show more anti-biased tendency than the ones which are selected by maximum circular velocity, confirming [23, 40]. Keeping these in mind, we take biased distribution for subhalos number density:

$$n_{sub} = 5.84 \text{ kpc}^{-3} \left(\frac{m_{cut}}{10^{6.5} M_\odot} \right)^{-a+1} \frac{\rho_h(r)}{M_\odot \text{ pc}^{-3}}. \quad (\text{A5})$$

With this normalization, the total mass and number of subhalos with tidal mass bigger than $10^{6.5}$ between ~ 30 kpc and r_h^{vir} in VLII simulation is within 5% from the value calculated with our model using best fit parameters.

Aquarius simulation Aq-A-1 [41] is another simulation which has parameters similar to VLII. Specifically, it has nominal mass resolution, $m_p = 1.71 \times 10^3 M_\odot$, host halo mass, $M_{50} = 2.523 \times 10^{12} M_\odot$, and host halo radius, $r_{50} = 433$ kpc. However, their number of subhalos with mass bigger than $\sim 10^7 M_\odot$ is approximately twice VLII's. We

discuss the modification to our results in Table I and Table II if we use Aquarius normalization.

From this procedure, we can find the number density of subhalos per unit luminosity after tidal stripping, dn_{sub}/dL . The number of photons that we receive from a single subhalo with luminosity L and line of sight (los) distance λ from us, for channel $ch = \gamma\gamma$ or γZ is given by (5). By folding (5) with dn_{sub}/dL , we can obtain the values in Table I and Table II. On the other hand, the contribution to the host's $\langle \rho^2 \rangle$ from subhalos is given by:

$$\langle \rho_{sub}^2 \rangle = n_{sub} \times \langle L \rangle, \quad (\text{A6})$$

where $\langle L \rangle$ is the average luminosity of the entire subhalos population after tidal stripping.

The anti-biased distribution is taken from appendix A of [24]. The normalization is such that the total mass in subhalos with masses between $10^{-5}M_h$ and $10^{-2}M_h$ is 3.4% of M_h . (In the original paper, the authors normalize to 10% of M_h . However, if we only include *bound subhalos*

within virial radius, the mass fraction is only 3.4%.) In this model, the authors encapsulates the tidal force from the host halo by adding radial dependence to the $m_{vir} - c_{vir}$ relation, so that subhalo closer to GC has higher concentration.

As a further refinement, we also add the Galactic disk to the VLII halo. For the Galactic disk model, we follow [35], for NFW parameter and our distance to GC, $R_\odot = 8.5$ kpc. We *spherically average the Galactic disk*. The relative difference in density between the averaged version and the original version is substantial only in the disk plane. There is no noticeable difference to the pericenter PDF, and the only modification to biased distribution is that, we replace $\rho_h \rightarrow \rho_h + \rho_{disk}$ in (A3). For anti-biased one, the effect of host tidal forces have been taken into account by adding radial dependence to the $c_{vir} - m_{vir}$ relation. Therefore, in eq. (A3), we replace $\rho_h \rightarrow \rho_{disk}$. We also use the same pericenter distribution as in the biased one.

-
- [1] C. Weniger (2012), 1204.2797.
 - [2] M. Su and D. P. Finkbeiner (2012), 1206.1616.
 - [3] E. Tempel, A. Hektor, and M. Raidal (2012), 1205.1045.
 - [4] A. Rajaraman, T. M. Tait, and D. Whiteson (2012), 1205.4723.
 - [5] W. Buchmuller and M. Garny (2012), 1206.7056.
 - [6] A. Boyarsky, D. Malyshev, and O. Ruchayskiy (2012), 1205.4700.
 - [7] M. Ackermann et al. (LAT Collaboration) (2012), 1205.2739.
 - [8] M. Kuhlen, J. Guedes, A. Pillepich, P. Madau, and L. Mayer (2012), 1208.4844.
 - [9] K. Rao and D. Whiteson (2012), 1210.4934.
 - [10] E. Charles, A. Albert, E. Bloom, S. A., Z. Yang, and G. Zaharijas, *4th fermi symposium, monterey ca* (2012).
 - [11] A. W. B. Albert, H. R., and E. Bloom, *4th fermi symposium, monterey ca* (2012).
 - [12] D. P. Finkbeiner, M. Su, and C. Weniger (2012), 1209.4562.
 - [13] D. Whiteson, JCAP **1211**, 008 (2012), 1208.3677.
 - [14] D. Whiteson (2013), 1302.0427.
 - [15] M. R. Buckley and D. Hooper (2012), 1205.6811.
 - [16] T. Cohen, M. Lisanti, T. R. Slatyer, and J. G. Wacker (2012), 1207.0800.
 - [17] I. Cholis, M. Tavakoli, and P. Ullio, Phys.Rev. **D86**, 083525 (2012), 1207.1468.
 - [18] A. Hektor, M. Raidal, and E. Tempel (2012), 1207.4466.
 - [19] M. Su and D. P. Finkbeiner (2012), 1207.7060.
 - [20] A. Hektor, M. Raidal, and E. Tempel (2012), 1208.1996.
 - [21] D. Hooper and T. Linden, Phys.Rev. **D86**, 083532 (2012), 1208.0828.
 - [22] J. Diemand, M. Kuhlen, and P. Madau, Astrophys.J. **657**, 262 (2007), astro-ph/0611370.
 - [23] J. Diemand, M. Kuhlen, and P. Madau, Astrophys.J. **667**, 859 (2007), astro-ph/0703337.
 - [24] M. Kuhlen, J. Diemand, and P. Madau, Astrophys.J. **686**, 262 (2008), 0805.4416.
 - [25] C. Evoli, D. Gaggero, D. Grasso, and L. Maccione, JCAP **0810**, 018 (2008), 0807.4730.
 - [26] <http://www.desy.de/~maccione/DRAGON/>.
 - [27] I. Cholis, M. Tavakoli, C. Evoli, L. Maccione, and P. Ullio, JCAP **1205**, 004 (2012), 1106.5073.
 - [28] M. Tavakoli (2012), 1207.6150.
 - [29] M. Tavakoli, I. Cholis, C. Evoli, and P. Ullio (2013), Diffuse Galactic Gamma Rays at intermediate and high latitudes. II. Constraints on the DM properties.
 - [30] I. A. Grenier, J.-M. Casandjian, and R. Terrier, Science **307**, 1292 (2005).
 - [31] T. F.-L. Collaboration (The Fermi-LAT Collaboration), Astrophys.J. **750**, 3 (2012), 1202.4039.
 - [32] T. Bringmann, X. Huang, A. Ibarra, S. Vogl, and C. Weniger (2012), 1203.1312.
 - [33] D. Merritt, J. F. Navarro, A. Ludlow, and A. Jenkins, Astrophys. J. Lett. **624**, L85 (2005), astro-ph/0502515.
 - [34] J. I. Read, G. Lake, O. Agertz, and V. P. Debattista (2008), 0803.2714.
 - [35] R. Catena and P. Ullio, JCAP **1008**, 004 (2010), 0907.0018.
 - [36] P. Salucci, F. Nesti, G. Gentile, and C. Martins, Astron.Astrophys. **523**, A83 (2010), 1003.3101.
 - [37] P. M. W. Kalberla, L. Dedes, J. Kerp, and U. Haud (2007), 0704.3925.
 - [38] A. M. Green, S. Hofmann, and D. J. Schwarz, Mon.Not.Roy.Astron.Soc. **353**, L23 (2004), astro-ph/0309621.
 - [39] S. Profumo, K. Sigurdson, and M. Kamionkowski, Phys.Rev.Lett. **97**, 031301 (2006), astro-ph/0603373.
 - [40] J. Diemand et al., Nature **454**, 735 (2008), 0805.1244.
 - [41] V. Springel, J. Wang, M. Vogelsberger, A. Ludlow, A. Jenkins, et al., Mon.Not.Roy.Astron.Soc. **391**, 1685 (2008), 0809.0898.
 - [42] P. L. Nolan et al. (Fermi-LAT Collaboration), Astrophys.J.Suppl. **199**, 31 (2012), 1108.1435.
 - [43] A. Drlica-Wagner, *Private communication* (2012).
 - [44] K. Gorski, E. Hivon, A. Banday, B. Wandelt, F. Hansen, et al., Astrophys.J. **622**, 759 (2005), astro-ph/0409513.

- [45] N. Arkani-Hamed, D. P. Finkbeiner, T. R. Slatyer, and N. Weiner, *Phys.Rev.* **D79**, 015014 (2009), 0810.0713.
- [46] M. Lattanzi and J. I. Silk, *Phys.Rev.* **D79**, 083523 (2009), 0812.0360.
- [47] J. Hisano, S. Matsumoto, and M. M. Nojiri, *Phys. Rev. Lett.* **92**, 031303 (2004), hep-ph/0307216.
- [48] J. Hisano, S. Matsumoto, M. M. Nojiri, and O. Saito, *Phys. Rev.* **D71**, 063528 (2005), hep-ph/0412403.
- [49] I. Cholis and L. Goodenough, *JCAP* **1009**, 010 (2010), 1006.2089.
- [50] T. R. Slatyer, N. Toro, and N. Weiner, *Phys.Rev.* **D86**, 083534 (2012), 1107.3546.
- [51] G. Dobler, D. P. Finkbeiner, I. Cholis, T. R. Slatyer, and N. Weiner, *Astrophys.J.* **717**, 825 (2010), 0910.4583.
- [52] T. A. Porter, I. V. Moskalenko, A. W. Strong, E. Orlando, and L. Bouchet, *Astrophys. J.* **682**, 400 (2008), 0804.1774.
- [53] A. Abdo et al. (The Fermi-LAT collaboration), *Phys.Rev.Lett.* **104**, 101101 (2010), 1002.3603.
- [54] <http://www.uchicago.edu/~diemand/vl/data.html>.
- [55] J. S. Bullock, T. S. Kolatt, Y. Sigad, R. S. Somerville, A. V. Kravtsov, et al., *Mon.Not.Roy.Astron.Soc.* **321**, 559 (2001), astro-ph/9908159.
- [56] H. Zechlin, M. Fernandes, D. Elsaesser, and D. Horns, *Astron.Astrophys.* **538**, A93 (2012), 1111.3514.
- [57] G. Tormen, A. Diaferio, and D. Syer (1997), astro-ph/9712222.
- [58] S. Kazantzidis, L. Mayer, C. Mastropietro, J. Diemand, J. Stadel, et al., *Astrophys.J.* **608**, 663 (2004), astro-ph/0312194.
- [59] E. Hayashi, J. F. Navarro, J. E. Taylor, J. Stadel, and T. R. Quinn, *Astrophys.J.* **584**, 541 (2003), astro-ph/0203004.
- [60] J. Gan, X. Kang, F. C. den Bosch, and J. Hou (2010), 1007.0023.
- [61] There have been 16 unassociated point sources in the 2yr *Fermi* catalogue detected at the level of $\simeq 4\sigma$ or more. In order to reach that significance a spectrum at low energies is also needed. DM does not give a strong spectrum signal at low energies so the actual spectrum of these sources (if they are DM subhalos) may be contaminated by other close-by point sources or diffuse γ -rays. That may also result in a non-trivial selection effect.
- [62] Our 4.4 yr sample refers to the data from 04 August 2008-03 January 2013.
- [63] This value is obtained assuming isotropic distribution. The actual distribution of the 111 and 129 GeV photons is not isotropic but rather peaks on the Galactic disk. Our results do not differ that much though since the distribution of the 575 unassociated point sources also peaks on the Galactic disk.
- [64] [19] suggest a p-value of $p = 0.00069$ for having 13 SOURCE events given a background described by a power-law.
- [65] The angular resolution of the *Fermi* LAT instrument is different at the energies we study by about a factor of 2 between the front and the back-converted photons. With $N_{\text{side}}=128$ our pixels include entirely the front-converted photons are slightly smaller than the 68% containment angle for back-converted events. Choosing $N_{\text{side}}=256$ would have resulted in photon events being spread in multiple pixels thus making them correlated; while $N_{\text{side}} \leq 64$, would be underestimating the ability of the instrument to resolve γ -ray structures at these energies. We have checked that our best fit results are consistent within 2% for N_{side} of 128, 64, 32, 16 and 8.
- [66] Since we use the entire 4π sky and have selected in advance the energy range of the γ -ray events based on the works of [1–6] there is no look elsewhere effect accounted for.